Egypt. J. Geo. **Vol. 68,** pp: 417 - 435 (2024)

Egyptian Journal of Geology

https://egjg.journals.ekb.eg

Integrating Remote Sensing, GIS, and Magnetic Geophysics for the Evaluation of Mineral Resources in the Bahariya-Farafra Region, Western Desert, Egypt, for Industrial Development

Alaa Nayef Hasan[1, *], Mostafa Nagy[2], Mohamed Anwar Ahmed[1] and **Ahmed El-Meselhy[3]**

[1] *National Authority for Remote Sensing and Space Sciences, Egypt*
[2] *Geology Department, Faculty of Science, Kafr Elsheikh University, Egypt*
[3] *Department of Geophysical Sciences, National Research Centre, Cairo, Egypt*

THIS STUDY integrates remote sensing, GIS, and aeromagnetic geophysical methods to evaluate mineral resources in the Bahariya-Farafra region, Western Desert, Egypt, to promote sustainable industrial development. The region is rich in various nonmetallic minerals and ornamental stones, including calcite, gypsum, clay minerals, sandstones, limestones, and dolomites, as well as significant iron ore deposits. Advanced edge detection filters and CET grid analysis were applied to aeromagnetic data to delineate geological structures, fault systems, and areas with potential mineralization. The results reveal promising zones for sulfide-bearing minerals, supported by identifying key lineaments associated with mineral accumulation. This comprehensive approach offers valuable insights for investment in strategic industries, enhances national income, and encourages urban development, contributing to alleviating population density issues in urban centers. The study underscores the importance of multi-disciplinary methodologies in resource assessment, laying the groundwork for future exploration and sustainable development initiatives in Egypt's Western Desert.

Keywords: Remote Sensing, GIS, Aeromagnetic Method, Mineral Exploration, Bahariya-Farafra Region.

1. Introduction

Bahariya and Bahariya-Farafra Road are the main morphotectonic depressions found in the Western Desert of Egypt. Bahariya Oasis is covered by a cretaceous–quaternary sedimentary sequence. The oldest rocks exposed in the Bahariya area are formed of quartz sandstones, sands, and clays of the bahariya formation of the lower Cenomanian age. This is unconformably overlain by El-Hamra, Qazzun, and Naqb formation of upper to middle Eocene, formed mainly of limestone (the host rocks of the known Bahariya iron ore). This is followed by the Radwan formation of the Oligocene age, consisting of sandstone, quartzitic sands, and quartzite (Youssef et al., 1970). Farafra Oasis covers an area of about 12000 Km2, forming an erratically triangular shape with the north and increasing in width to the south. It can be described as a generally low-lying depression of almost flat Poor in the order of 100 m elevation. It is surrounded by a topographic contour line of 200 m above sea level. The Farafra Depression is bordered by cliffs on three sides. The eastern and western cliffs are notably bold and reach impressive heights, while the northern cliff, though shorter, stands out with its strikingly white, precipitous face. it is backed at some distance by another cliff. The distance between the eastern and western cliffs in

*Corresponding author e-mail: alaa_nayef@hotmail.com
Received: 07/11/2024; Accepted: 09/11/2024
DOI: 10.21608/EGJG.2024.334656.1093

the latitude of Qasr Farafra is about 90 km., whereas the total length from the Dakhla escarpment to the apex of the Farafra depression in the north is about 200 kilometers. The depression floor of Farafra Oasis is cut in a white chalk bed, which is a part of an extensive mappable rock unit known in the literature as the chalk. This unit covers large tracts of the southern part of the Western Desert and belongs to the Maastrichtian age (Le Roy, 1953; Said and Kerdany, 1961). North of the latitude of Bir Dikkar, the floor of the Farafra depression varies little in general level and has no marked peculiarities except for some conspicuous and isolated conical hills on the western side. The geology of Bahariya and Farafra depressions comprises a wide range and different types of Phanerozoic sedimentary deposits make these depressions a valid geological environment for metallic and nonmetallic ore minerals occurrences.

Geophysical techniques have been extensively utilized to identify rock units and structural features that may influence the occurrence of metal mineralization (Eldosouky et al., 2017; Chattoraj et al., 2020; Elkhateeb et al., 2021; Adebiyi et al., 2024). Among these, aeromagnetic data offer several distinct advantages over other geophysical methods, including rapid spatial coverage and affordability per unit area, which make them particularly suitable for detecting concealed ore bodies and structural anomalies such as faults, dykes, and shear zones that are often associated with mineral deposits (Eldosouky et al., 2018; Ekwok et al., 2022; Eldosouky et al., 2024). Metallic mineralization is commonly related to structural features and hydrothermal alterations induced by magma intrusions (Xu et al., 2016). Significant progress has been made in the processing and enhancement of magnetic data, as well as in the interpretation techniques, enabling the automatic detection of linear structures and porphyry magnetic signatures that may influence mineralization. These advancements complement traditional methods and provide enhanced capabilities for exploration (Cordell and Grauch, 1982; Miller and Singh, 1994; Cooper, 2003; Holden et al., 2008; Shebl, 2021).

Additionally, airborne magnetic surveys have recently been chosen in numerous studies for plotting variations in magnetization caused by hydrothermal alterations in igneous rocks (Abedi et al., 2013; Eldosouky and Elkhateeb, 2018; Magbo and Eze, 2024). Thus, we employed aeromagnetic methods as a tool for mineral assessment to identify magnetization differences between rock types, geological contacts, fractures, faults, dykes, and rock boundaries.

Therefore this study's principal goal is to propose a viable model for predicting new locations of sulfide-bearing zones through a combination of remote sensing, and geophysical analyses.

1.2. Geological settings

The Bahariya Depression, located in the central region of Egypt's Western Desert (Fig. 1), is elongated and encircled by a prominent carbonate plateau. In the northern section, the stratigraphic sequence contains the Bahariya Formation (Early Cenomanian), Hefuf Formation (Campanian), and El Heiz Formation (Late Cenomanian) and, which collectively constitute the depression base. These formations are bordered by Eocene carbonate rocks (El Akkad & Issawi, 1963; Said & Issawi, 1964). The Eocene carbonate rocks, beginning with the Naqb Formation, rest unconformably on top of the Upper Cretaceous Bahariya Formation's siliciclastic deposits (Figs. 1, 2) (Said, 1962; Afify et al., 2015a). The Naqb Formation is then overlain by the Qazzun and El Hamra formations, which are shown with reduced thickness in the northeastern sector (Figs. 1, 2). Ironstone deposits are spatially associated with Eocene carbonates at three major sites (Fig. 1). The Radwan Formation's Oligocene ferruginous quartzarenite layers unconformably cover the Eocene units and the ironstone layers (Figs. 1, 2). In the northern portion of the depression, as well as farther south, are outcrops of Middle Miocene basaltic and doleritic igneous dykes, sills, laccoliths, and lava flows (El-Etr & Moustafa, 1978; Meneisy, 1990). There are two main types of these alkaline basaltic formations: dolerite and olivine basalt (Meneisy, 1990).

Along with several doubly plunging folds and extensional faults, the Bahariya Depression is structurally influenced by a northeast-trending, right-lateral wrench fault system (Fig. 1) (Sehim, 1993; Moustafa et al., 2003). Three main stages of structural deformation have occurred in the northern portion of the depression: (1) right-lateral transpression orientated towards ENE from the post-Campanian to pre-Middle Eocene, (2) tectonic reactivation from the post-Eocene, and (3) Middle Miocene extensional deformation (Moustafa et al., 2003). Through the cumulative effects of the first two deformation phases, the Bahariya swell was

formed during the initial transpressional regime (Said & Issawi, 1964). With structural resemblances to the Esna Formation (Paleocene–Early Eocene) in the northern Farafra region, the stresses during this phase produced NE-SW orientated doubly plunging anticlines and ENE-oriented strike-slip faults that.

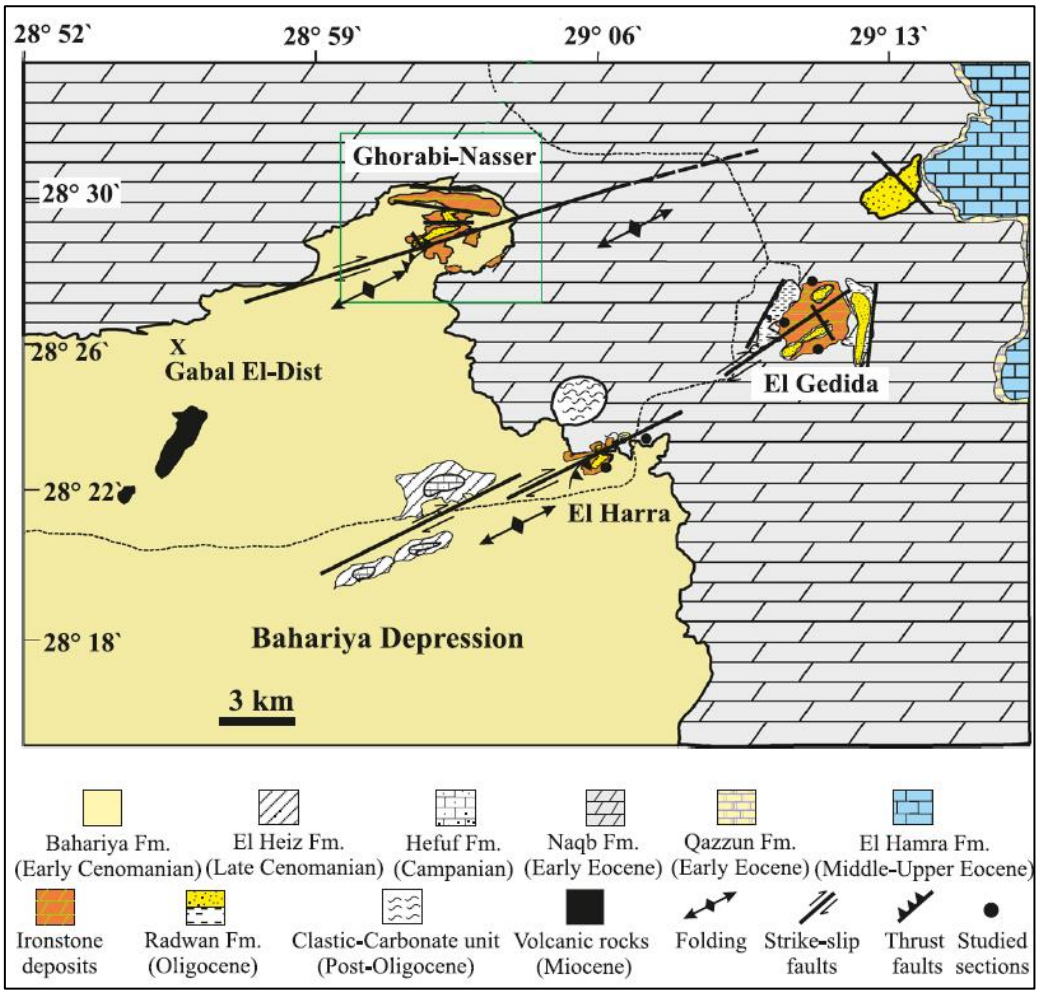

Fig. 1. Geologic map of the northern Bahariya Depression (modified after Moustafa et al., 2003).

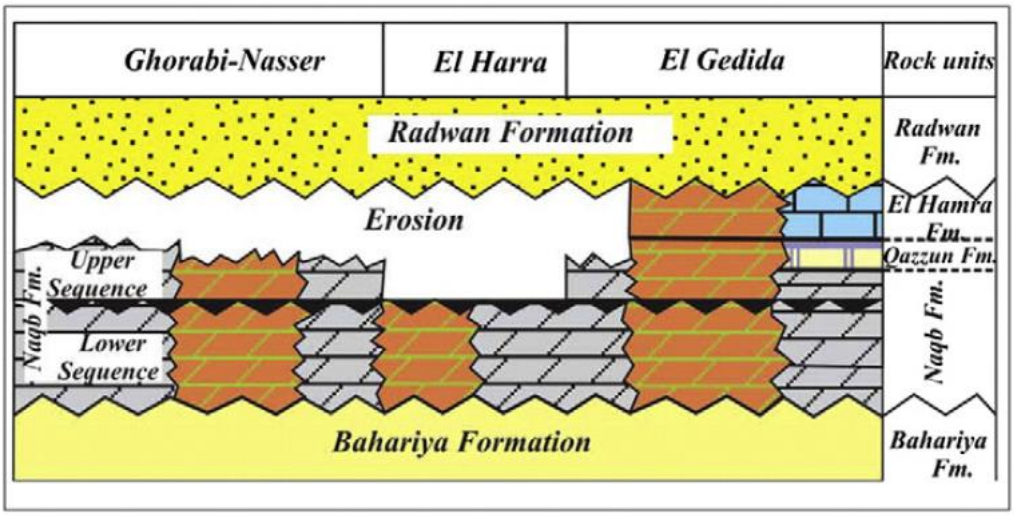

Fig. 2. Geologic profile showing the stratigraphic succession exposed in the northern part (Afify et al., 2015).

Lasted throughout the Paleocene and Eocene (Sanz-Montero et al., 2013; El Ayyat, 2013). Additionally, Eocene sedimentation in Bahariya and Farafra was impacted by syndepositional tectonics and seismic pulses. The Farafra region In Bahariya and Farafra, syndepositional tectonics and seismic pulses also had an impact on Eocene sedimentation (Said & Issawi, 1964; Obaidalla et al., 2006).

Tectonic inversion and the development of folds and small domes within Eocene formations were features of the second tectonic phase, which took place between the Middle Eocene and Oligocene (Said & Issawi, 1964; Moustafa et al., 2003). The carbonate sequence was broken and folded by this phase along right-stepped, NE to ENE orientated en-échelon folds (Fig. 1). Prominent dextral strike-slip faults orientated NE-SW, localised thrusts close to folded regions (such as southern Ghorabi and El Harra) (Fig. 1), E-W normal faults, WNW-oriented, and left-stepped en-échelon normal faults. Many of these faults were mainly linked to the Middle Miocene extensional deformation and had an effect on the Oligocene Radwan Formation. Along structural fissures and discontinuities, erupted or intruded materials indicate volcanic activity associated with this phase. The opening of the Gulf of Suez-Red Sea rift, which separated Arabia from Africa, most likely corresponds to this extensional regime (Moustafa et al., 2003). The main events influencing the carbonate plateau formations in the Bahariya region were the second and third tectonic phases.

3. Materials and methods

3.1. Remote sensing data

Remote sensing images can be used for mineral exploration for different purposes e.g. (1) mapping geologic features, Faults and fractures serve as primary controls in the localization of ore deposits, while hydrothermally altered rocks can be distinguished by their unique spectral signatures. Landsat Thematic Mapper (TM) satellite imagery is extensively utilized for the interpretation of structural features and hydrothermal alterations. Through digital processing, TM ratio images effectively detect two principal assemblages of hydrothermal alteration minerals: iron oxides and an assemblage of clays with alunite (Floyd, 1999).

Remote sensing has revolutionized mineral exploration by providing detailed spectral data that helps geoscientists identify mineral deposits based on their unique spectral signatures. In the present study, the following methods and techniques are used:

1. **False Color Composite (FCC):** This technique involves combining multiple spectral bands to create images that reveal specific mineralogical features. For example, in mineral-rich areas, FCC images can highlight altered minerals associated with hydrothermal activity, as seen in near-infrared and shortwave-infrared bands. Such combinations allow minerals to appear in distinct colors, making it easier to detect hydrothermally altered zones, which are potential indicators of mineral deposits.
2. **Principal Component Analysis (PCA)**: PCA is widely used in remote sensing to reduce data redundancy and emphasize spectral features relevant to mineral exploration. By isolating principal components that capture the variance of specific minerals, geologists can enhance the visibility of alteration zones related to mineralization. This method can reveal mineral anomalies like iron oxides and hydroxyl-bearing minerals, which are often associated with ore deposits.
3. **Band Ratio Technique:** Band ratios are simple mathematical operations between spectral bands that highlight specific minerals by enhancing their reflectance or absorption features. For example, certain band ratios are useful for identifying iron oxides or hydroxyl minerals, which signal alteration zones indicative of possible ore deposits. By selecting bands that target specific minerals' unique spectral responses, band ratios are effective for quick mineral identification.
4. **Supervised Classification: Spectral Angle Mapper (SAM):** SAM is a classification method that compares the spectral signature of pixels to reference spectra. This approach is useful in identifying specific minerals in multispectral or hyperspectral data. SAM assigns each pixel a class based on its spectral similarity to known mineral spectra, enabling detailed mineral mapping over large areas
5. **Constrained Energy Minimization (CEM):** This technique emphasizes specific target minerals while minimizing interference from other materials. CEM is particularly useful for mineral exploration in complex geological settings where multiple minerals might have

overlapping spectral features. It helps focus on particular mineral signatures, improving accuracy in detecting valuable mineral deposits

3.2. Aeromagnetic data

The primary collection of aeromagnetic data yielded a total magnetic intensity (TMI) map with a geographical inclination of 41.5° North and a declination of 1.86° east, as recorded by Aero Service in 1984. This raw TMI map underwent a digitization process and was subsequently transformed into an x, y, and z file. The Geosoft software package was employed to grid this file, generating the TMI grid. The final TMI map is presented at a 1:50,000 scale, as shown in Fig. 13.

As described in (Spector and Grant, 1970), a critical processing step was performed on the gridded total magnetic map using the Fourier transform algorithm. As a result, a map that was scaled down to the north magnetic pole was produced, which successfully placed the magnetic anomalies over their respective sources. In order to perform a thorough structural complexity analysis of the region being studied, this reduced-to-pole (RTP) data was crucial.

3.2.1 High-precision edge detection

To identify faults, contacts, dykes, and ore deposits, edge detection is a popular geophysical exploration technique (Eldosouky et al., 2022b; Abuzied et al., 2024; Eldosouky et al., 2024). Since the main goal is to accurately map the boundaries of causative sources and structures, these techniques are an essential step in the interpretation of potential field data (Nasuti et al., 2019; Arafa et al., 2020; Pham, 2023; Pham et al., 2023; Othman and Ibraheem, 2024). Six improved techniques have been adopted and used to analyse the data for mapping magnetic boundaries in order to look into the structural influences related to the location of ore deposits.

The TDY filter was developed by Nasuti et al. (2018) to enhance the detection of anomalous edges. This filter balances noise and the filtered signal while enhancing anomaly edges of different magnitudes and depths. A more quantitative interpretation of possible field data maps is made possible by the TDY filter, which makes the shapes of the anomalies clear and highlights hidden anomalies that are missed by other traditional filters. Additionally, this filter isolates neighbouring bodies and highlights both shallow and deep anomaly edges. The positive and negative anomalies and the anomaly edges are indicated by the filter's maximum, minimum, and zero values, respectively. The formula provided by Nasuti et al. (2018) was used to calculate the TDY and THD-TDY filters.

Similarly, Nasuti and Nasuti (2018) proposed the NTilt filter to improve the delineation of geological source edges derived from potential field data. This filter uses the vertical derivative of the analytical signal in varying orders to equalize signals from sources buried at different depths. The NTilt filter provides a superior edge definition of causative anomalies and improves the accuracy of outlining deep-seated anomalies compared to other techniques. It offers increased precision and sharper edge detection, more effectively distinguishes nearby anomalies, and reduces the likelihood of generating false edges, thereby minimizing potential field interpretation ambiguity. This filter shows promise in delivering a higher-quality qualitative interpretation of magnetic data compared to more commonly used filters. The maximum filter value highlights the edges of anomalous magnetic bodies. The formulation of the NTilt and THD_NTilt filters is based on the equations provided by Nasuti and Nasuti (2018).

The impTDX filter, a sophisticated horizontal tilt angle filter created to maximise source boundary detection, was presented by Ibraheem et al. in 2023. This filter produces clearly defined boundaries at different depths by normalising second-order vertical derivatives (SVD) using the hyperbolic tangent function. In comparison to other filters, it improves the differentiation of nearby anomalies, lessens the likelihood of false edges, and shows less sensitivity to noise. The response of the impTDX filter varies between -1 and 1, peaking above the whole source body. Furthermore, to attain maximum values along source edges, Ibraheem et al. (2023) recommend computing the THD of the impTDX filter (THD_impTDX). Ibraheem et al. (2023) provided formulas that were used to derive the impTDX and THD_impTDX filters.

3.2.2 CET Grid Analysis

The CET method is a fairly novel approach encompassing automated tools for interpreting texture, lineation, structural complexity, and

pinpointing potential mineralized regions, as stated in (Holden et al., 2008). This technique offers two distinct strategies for automatic lineament delineation: image enhancement based on texture analysis and detection of discontinuity structures. As part of our study, we applied texture analysis-based image enhancement that emphasizes variations in local intensity and enhances areas of discontinuity to help identify junctions, intersections, and strike direction changes. The extraction of tectonic patterns from magnetic signals involves three stages: 1) the magnetic data (RTP) is transformed into a standard deviation map to identify areas with complex textures. 2) Phase symmetry for locating zones of discontinuity formed by lateral continuous lines, using the textural analysis results. 3) Structure detection utilizing the phase symmetry outcomes to simplify areas with discontinuities into skeletal structures, represented as a binary grid. Following the application of a structure detection workflow to

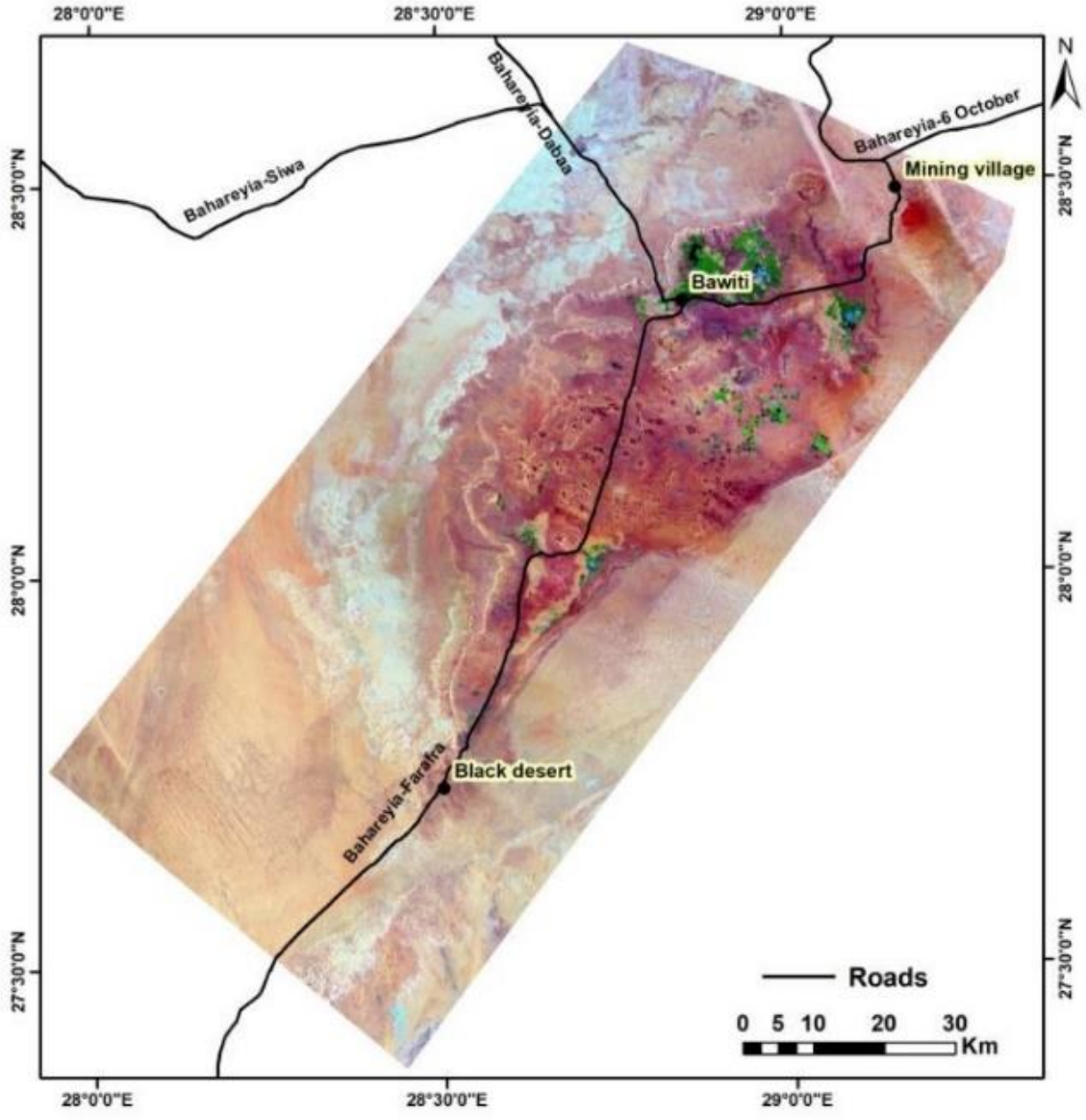

Fig. 3. False color composite 7, 5 and 3 in RGB of Bahariya area.

form a database of identified, skeletonized, and vectorized features, an entropy heat map is produced. This map aids in identifying the most likely locations of ore deposits within the study area (Holden et al., 2012; Eldosouky et al., 2020a; Shebl, 2021; Uwiduhaye et al., 2021).

4. Results and discussion

4.1. Interpretation of Remote sensing data (for Bahariya area)

4.1.1. False color composite

The best RGB band triplet for displaying the study area's structural and geological features is 7-5-3. A solid foundation for geological mapping is provided by this combination, which improves the differentiation of different exposed rock units (Fig. 3). Nanotechnology Lab in Agricultural Research Center, in Giza.

4.1.2. Principal Components Analysis (PCA)

The PCA technique was used for the Bahareyia area, and the analysis of the Eigenvector matrix (table 1) revealed that the first four bands contain 99.998% of the information variance of the data**,** making them the most informative bands. However, only 0.002% of the data is contained in the other bands. Therefore, the best PC colour composites for effective discrimination of all the rock units and agricultural areas encompassing the study area are PC3, PC2, and PC1 and PC4, PC3, and PC2 (Figs. 4 & 5). There are marked limestone plateaus in the first PC composite image by red color which is covered in some places by sandy deposits that are shown together with the dunes and sand sheets the yellow color, ferruginous rocks are shown in cyan color and the agricultural areas are in pink. In the second PC composite Image, limestone plateaus are marked by yellow to orange colors which is covered in some places by sandy deposits that are shown together with the dunes and sand sheets by the light blue color, ferruginous rocks are shown in dark blue color and the agricultural areas are in green.

Table 1. Eigenvector matrix and the loadings of principal components on landsat 8.

Eigenvector	Band1	Band2	Band3	Band4	Band5	Band6	Band7
Band1	-0.9352	0.322069	-0.05202	0.073682	-0.11585	-0.00868	-0.00624
Band2	-0.24005	-0.80429	-0.53136	0.086087	-0.01136	0.071429	0.02279
Band3	0.214887	0.44907	-0.69727	0.494679	0.140955	0.02635	-0.02648
Band4	-0.00195	0.200083	-0.41508	-0.8374	0.210979	0.204503	-0.00977
Band5	0.146491	0.079656	-0.17803	-0.11857	-0.95978	0.065269	-0.03163
Band6	0.008848	0.009613	-0.15359	-0.15626	-0.02325	-0.9217	0.318992
Band7	0.007515	0.03554	0.034473	0.052309	-0.01861	0.31388	0.946514
Eigenvalues	**0.002966**	**0.000006**	**0.000002**	**0.000001**	**0.000000**	**0.000000**	**0.000000**
% information	**99.697**	**0.203**	**0.068**	**0.03**	**0.002**		

4.1.3. Band ratio technique

For the Bahareyia area, two band ratio composite images were prepared; the first is ratio 3/1 in red, 5/4 in green, and 5/7 in blue; and the second ratio is ratio 5/7 in red, 3/5 in green and 3/1 in blue. The used ratio composites yielded good insight into rock units and agriculture. In the first ratio composite; the limestone plateaus are marked by light blue color which is covered in some places by sandy deposits that are shown together with the dunes and sand sheets by a light yellow color, ferrugenous rocks are shown in black color and the agricultural areas are in bright blue color (Fig.6). In the second ratio composite; the limestone plateaus are marked by light green color which is covered in some places by sandy deposits that are shown together with the dunes and sand sheets by the light blue color, ferrugenous rocks are shown in red color and the agricultural areas are in bright green (Fig.7).

4.1.4. Supervised classification: Spectral Angle Mapper (SAM)

The SAM result of the applied spectral measurements showed the spatial distribution of the areas having similar signatures like the input ones of the measured samples taken during the field work in Bahareyia-Heiz area (Fig. 8). The extension of similar signatures resulted by using this classification suggest the distribution of these rocks which is highly compared to geologic map of the

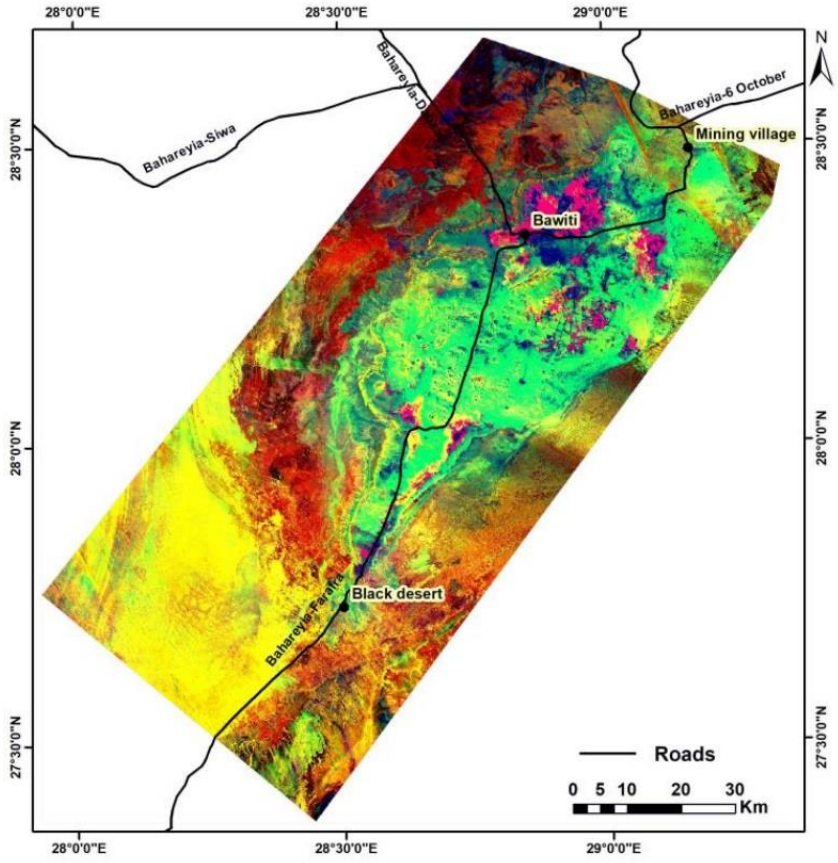

Fig. 4. PC3, PC2 and PC1 in RGB, respectively of Bahariya area.

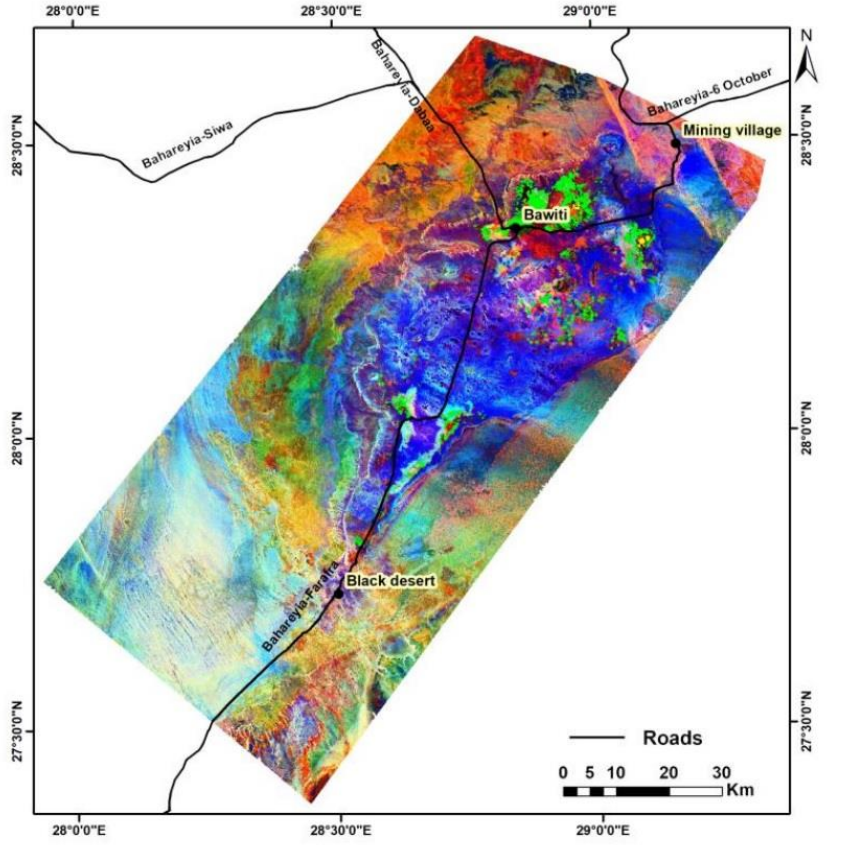

Fig. 5. PC4, PC3 and PC2 in RGB, respectively of Bahariya area.

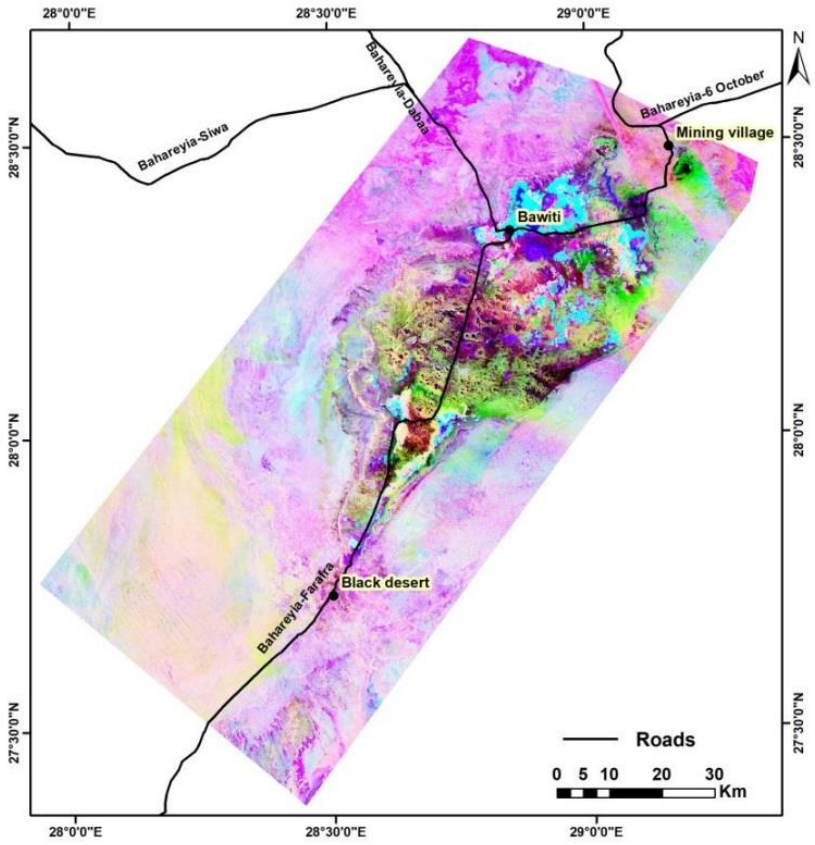

Fig. 6. Color ratio composite image (3/1, 5/4, 5/7) in RGB for Bahariya area.

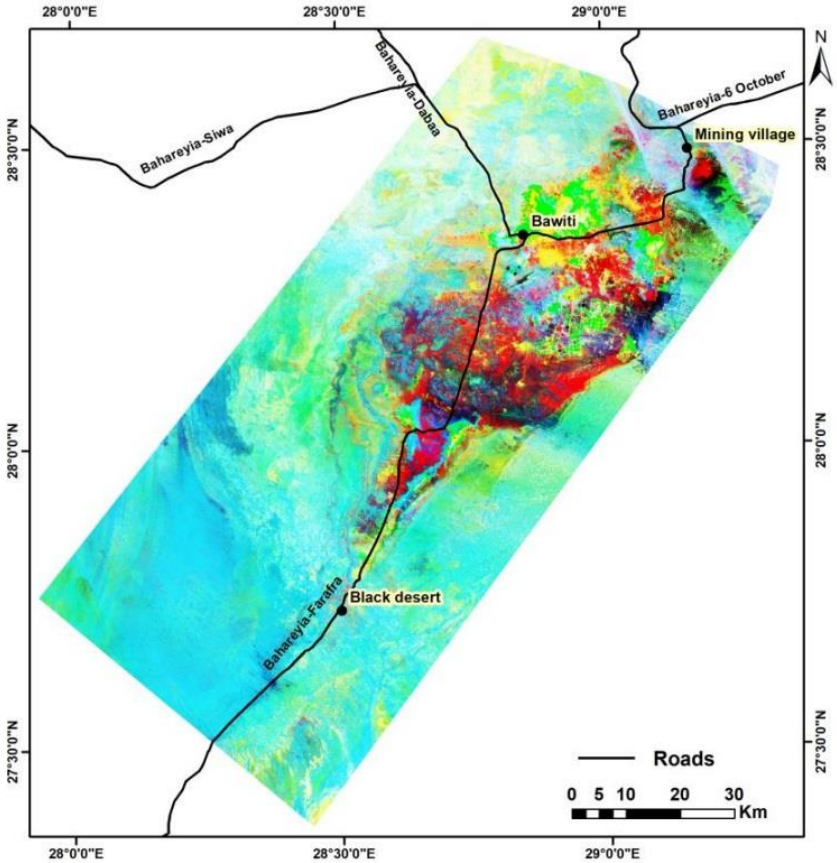

Fig. 7. Color ratio composite image (5/7, 3/5, 3/1) in RGB for Bahariya area.

area, ensuring the effectiveness and efficiency of this technique (Fig. 8).

In the resulted SAM classification image of the Bahareyia-Heiz area, the limestone plateaus are marked by greyish blue color which is coverd in some places by sandy deposits that are shown together with the sand dunes and sand sheets by the yellow color, ferrugenous rocks are shown in orange color, the agricultural areas are in bright green color and areas with high enrichment in iron are shown in red color (including bahareyia iron occurrences (El-Gedida, Ghorabi, Nasser and El Harra) and El Heiz ferruginous quartizitic sandstone in the isolated hills) (Fig. 9).

4.1.5. Constrained Energy Minimization (CEM)

The CEM result shows the spatial distribution of the areas having similar spectral signatures like the input ones of the targeted minerals from USGS, suggesting their localities and spatial extension, highlighted in different colors. This abundance of images shows that the distribution of clay minerals dominates in areas of agriculture (Fig. 10), Gypsum is found present near areas dominated by agriculture, these areas are of abundant clays and the field survey demonstrated the presence of gypsum as crack filling in the shales and clays (Fig.10).

Carbonate minerals are present in the area of the limestone plateaus and scarps, this sounds logic (Fig. 11). Iron oxides are abundant over the whole sector of the study area, they are found in the north eastern part of the Bahareyia area; in the mining area including bahareyia iron occurrences (El-Gedida, Ghorabi, Nasser and El Harra) and in the central part of the area in the caps of El Heiz isolated hills that are mainly formed of ferruginous quartizitic sandstone and ferruginous quartizitic claystone (Fig. 12).

4.2. Interpretation of Geophysical data

4.2.1. Aeromagnetic results

The RTP map of the study area reveals that the magnetic anomalies observed in the TMI map have been shifted northward (Fig. 13.A). This shift occurs due to the correction applied to the Earth's magnetic field's inclination and declination, which repositions the anomalies to their true locations. The RTP map demonstrates the combined influence of magnetic susceptibility variations in different rock types and geological structures spanning from deeper subsurface layers to the surface. This is evident through the changes in magnetic response, which result from both the composition of the subsurface materials and the structural features at varying depths.

The analysis of magnetic anomaly patterns and signatures allowed for the detailed interpretation of subsurface geological features, including the identification of magnetite-rich rocks, the estimation of basement depth, and the determination of the locations of subsurface structures (Lowrie, 2007). These anomalies provide critical insights into the distribution of magnetic minerals and the structural configuration beneath the surface, enabling a more accurate understanding of the geological framework.

Magnetic anomalies provide information about the distribution of magnetic minerals within various rock types when basement rocks are covered (Alexander et al., 2015). Evidence of possible mineralisation sites can be found in the variations in magnetic fields associated with fault zones and fractures. The geometry of the causative body, the declination and inclination of the body's magnetisation, the declination and inclination of the local Earth's magnetic field, and the body's orientation with respect to magnetic north are the main factors that determine the shape of a magnetic anomaly (Nabighian et al., 2005).

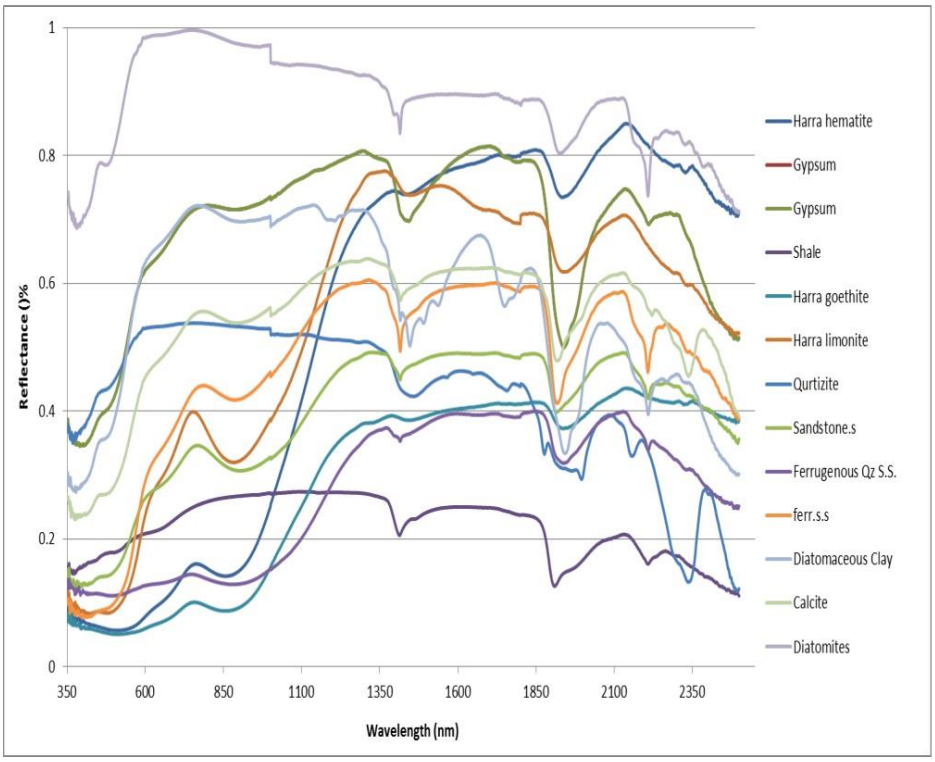

Fig. 8. Showing selected signatures of the measured samples.

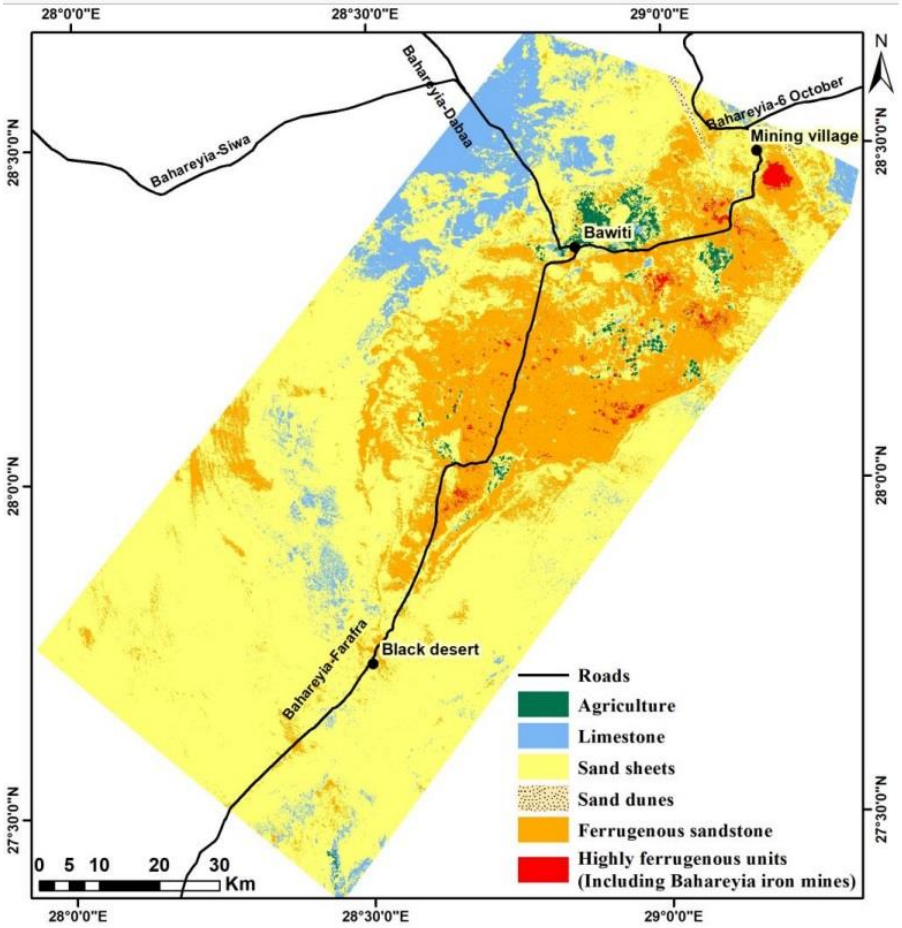

Fig. 9. SAM classification showing the different rock units in Bahariya area.

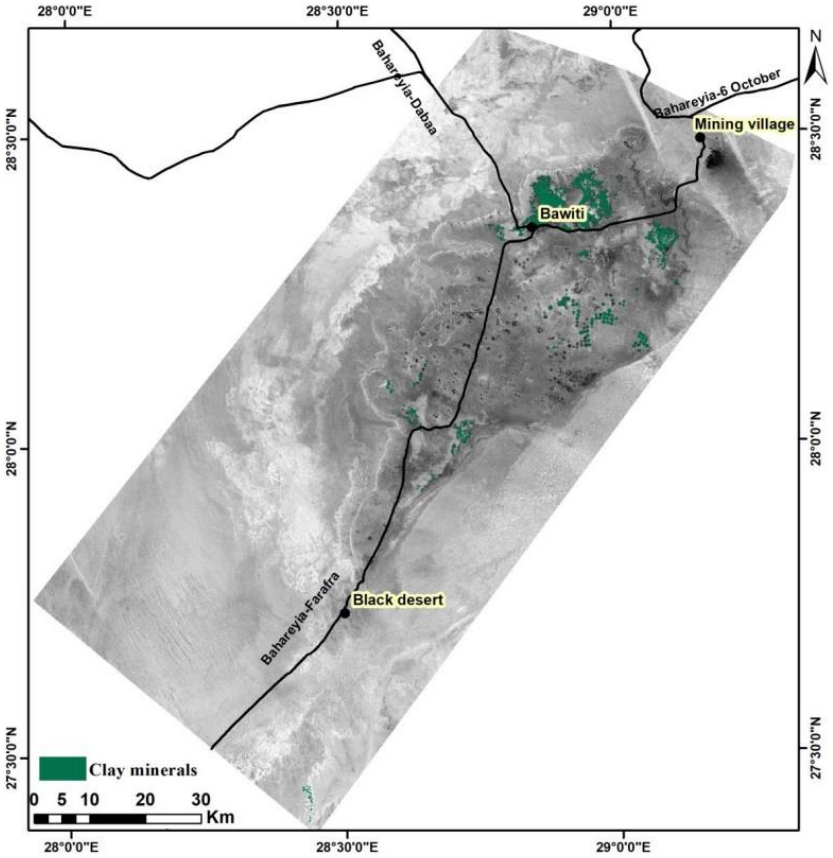

Fig. 10. The spatial distribution of clay minerals.

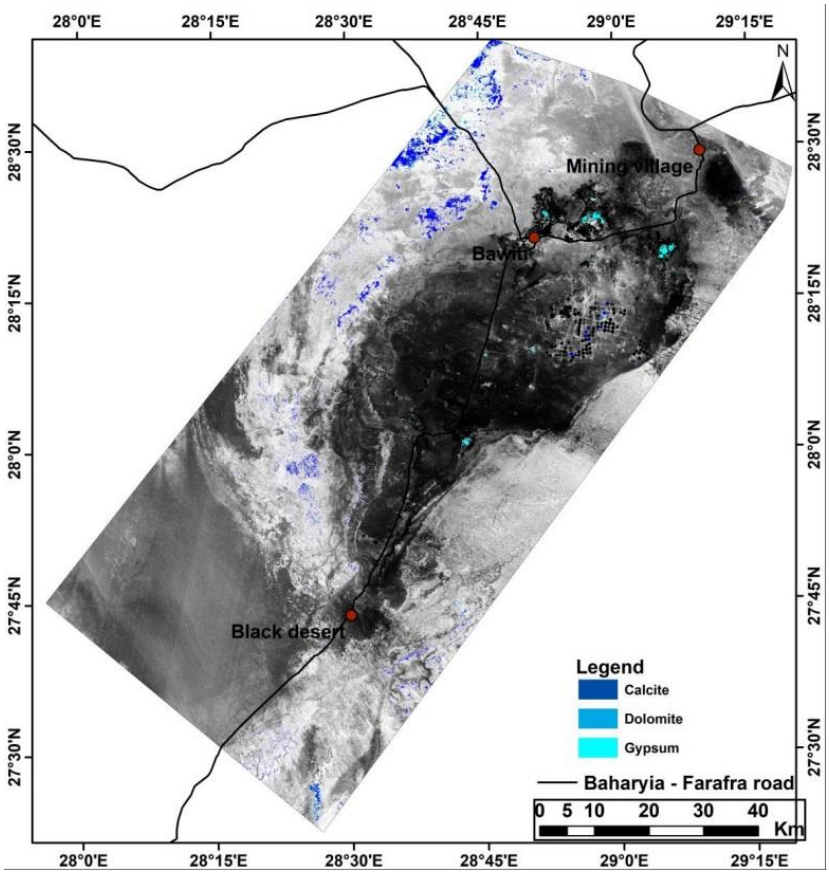

Fig. 11. The spatial distribution of Gypsum and carbonate minerals.

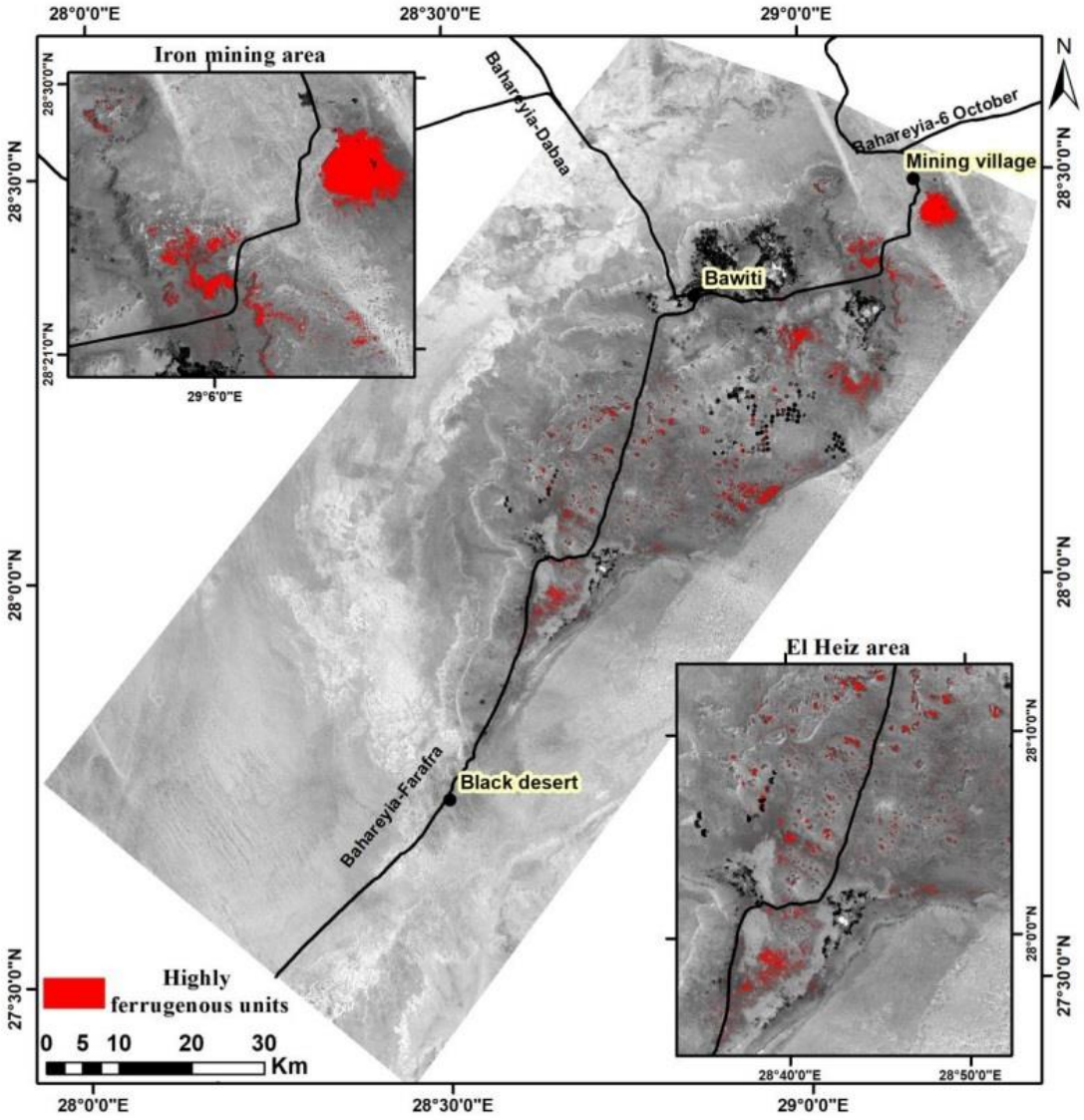

Fig. 12. The spatial distribution of Iron-rich rocks and highly ferruginous units.

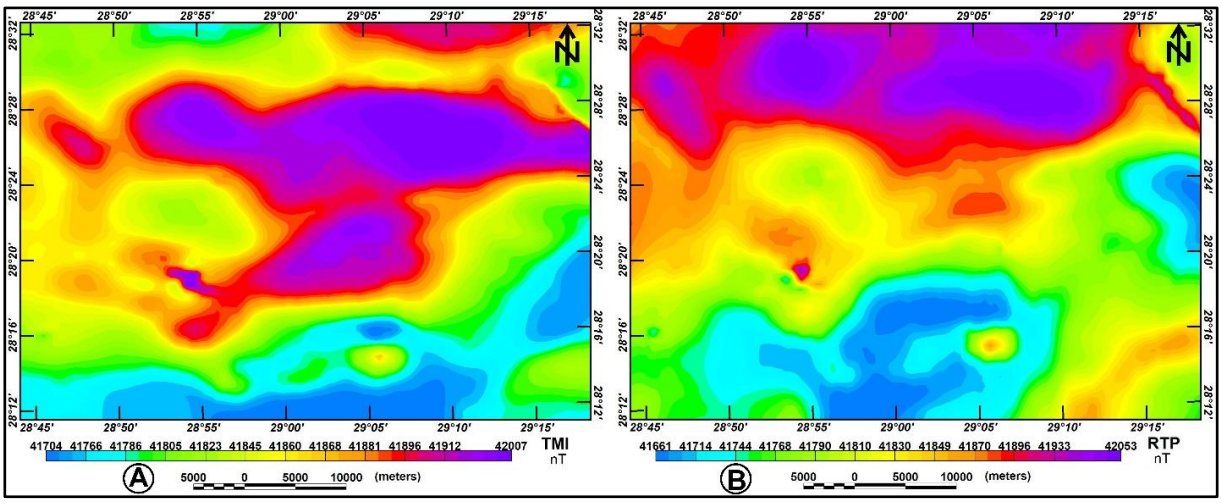

Fig. 13. (A) The total magnetic intensity map. (B) The reduced-to-pole (RTP) map of the study area.

The RTP map for the study area shows that the northern and northwestern sections are characterized by positive magnetic anomalies, whereas the southern and eastern regions are dominated by magnetic low anomalies (Fig. 13.B). The RTP map of the study area displays magnetic anomalies ranging between 41661 and 42053 nano Tesla. The high magnetic anomalies display a range of shapes, from ovoid to elongated, and are predominantly located in the northern and northwestern parts of the map. They extend in the N-W and E-W directions and have amplitudes ranging from about 41850 to about 42053 nano Tesla. The low magnetic anomalies, on the other hand, dominate the southern and eastern parts with amplitudes ranging from 41661 to 41750 nano Tesla and take irregular shapes and stretch in NE-SW and NW–SE directions (Fig. 13.B).

4.2.2. Regional-residual separation

The magnetic signatures observed in any RTP anomaly map reveal overlapping anomalies originating from different sources. Regional anomalies, identified by their long wavelengths, are associated with deep-seated, large geological bodies or structures. These regional features are crucial for studying significant tectonic elements, such as oceanic ridges and subduction zones. In contrast, residual anomalies, marked by shorter wavelengths, are linked to shallow geological formations with considerable significance (Lowrie, 2007).

Exploration geophysicists prioritize isolating residual anomalies, as these are crucial indicators for detecting mineral resources, water reservoirs, hydrocarbon traps, and other shallow geological features of interest. A residual magnetic grid can be generated by removing the regional magnetic influence, highlighting the effects associated with localized structures (Griffin, 1949) (fig.14).

4.2.3. High-precision edge detection

Edge detection techniques are essential tools in mineral exploration as they assist in mapping the shapes of magnetic source bodies and geological structures, which control the distribution of mineral deposits. Six high-precision edge detection filters were used in this investigation to locate and delineate magnetic source boundaries. TDY, NTilt, and impTDX are among them (shown in Fig. 15), as are THD-TDY, THD-NTilt, and THD-impTDX (shown in Fig. 15. A, B, and C, respectively).

Notably, zero-contour values highlight the edges of magnetic sources in the TDY, NTilt, and impTDX maps. These correspond to the peaks or maxima that the three additional filters found, as shown in Figure 16. Based on the produced maps, these filters prove highly effective at delineating subsurface bodies and structures compared to conventional methods. As a result of their high resolution, these filters can detect and distinguish various detailed anomalies resulting from weakly and strongly magnetized sources. These anomalies are difficult to distinguish on the RTP map, particularly in the central and southern portions of the study area.

The TDY (Fig. 15A) and THD-TDY (Fig. 16A) filters were especially well-suited for producing a comprehensive structure map because they showed distinct gradients along magnetic source boundaries. The edge detection of nearby causative anomalies linked to other popular filters is improved by the NTilt (Fig. 15B) and THD-NTilt (Fig. 16B) filters. These filters also effectively enhance edge sharpness while reducing false edges, which significantly lowers data interpretation ambiguity (Nasuti and Nasuti, 2018). Consequently, these filters offer a purer and more refined depiction of the structural framework, allowing for more detailed insights into subsurface features.

The NTilt (Fig. 15 B) and THD-NTilt (Fig. 16B) filters enhance the edge detection of adjacent causative anomalies related to other common filters. These filters also successfully enhance edge sharpness and reduce false edges, which significantly lowers data interpretation ambiguity (Nasuti et al., 2018). Consequently, these filters offer a richer and other refined depiction of the structural framework in the study area, allowing for more detailed insights into subsurface features.

The impTDX (Fig. 15 C) and THDR_impTDX (Fig. 16C) filters demonstrate exceptional accuracy in identifying source boundaries. They produce clearer and more refined boundaries and effectively delineate boundaries surrounding adjacent anomalies. This makes them highly effective for detailed structural mapping and distinguishing closely spaced features. These filters offer several benefits, including their ability to reduce false edge

detection and their greater resistance to noise compared to other commonly used filters. This leads to a significant reduction in uncertainty during result interpretation, providing more reliable and accurate data for analysis. The impTDX filter produces values between -1 and 1, derived from the hyperbolic tangent function, with the maximum values corresponding to the entire source body (Ibraheem et al., 2023). This range enables a better definition of the source body boundaries, contributing to a clearer geophysical interpretation. Since the THDR_impTDX filter can produce maximum values along the edges of magnetic sources, it was used to detect these boundaries precisely and obviously.

Based on the filter results, the maps reveal prominent magnetic trends in the NW-SE and NE-SW directions, with less pronounced trends in the E-W and N-S directions. The strong similarities observed across the TDY, THD-TDY, NTilt, THD-NTilt, impTDX, and THDR-impTDX maps contribute to a reduction in data uncertainty, enhancing the overall reliability of the magnetic interpretations. Furthermore, our findings are in good harmony with previous studies, including those by Rabeh et al. (2018) and El-Hussein and Shokry (2020). This agreement validates our analysis and results' reliability.

4.2.4. CET Grid Analysis

Magnetic data was subjected to the CET method in order to eliminate lineaments and linear features. The RTP data from the study area was subjected to the CET method. In order to identify the regions with complex textures linked to discontinuities in magnetic data, the standard deviation (STD) was calculated as part of the procedure (Fig. 16A). A phase symmetry map (PS) was then created using the STD output (Fig. 16B), which aids in locating possible areas of interest and differentiating continuous linear structures. This approach effectively separates these structures laterally, improving the clarity of the interpreted features. The size and orientation of the identified features are influenced by the chosen scale and orientation parameters. In this study, we utilized all orientations at the smallest scale that the Oasis Montaj V. 8.3 software permits (1000 meters) to capture the widest range of detected structures. It should be noted that the analysis only took into account positive features, such as the dykes' constant positive magnetic response. Line segments were extracted from the data using skeletonization and vectorization techniques in order to automatically detect linear structures in the study area (Fig. 16C). These procedures made it easier to more clearly and methodically highlight the features that were found.

A detailed examination of the vectorization map reveals prominent structural trends oriented NW-SE and NE-SW, with additional minor lineaments aligned along the N-S and E-W directions (Fig. 16C). These lineaments likely represent fractures, faults, contacts, or edges of magnetized subsurface bodies and are considered potential sites for mineral accumulation. These structural features are vital

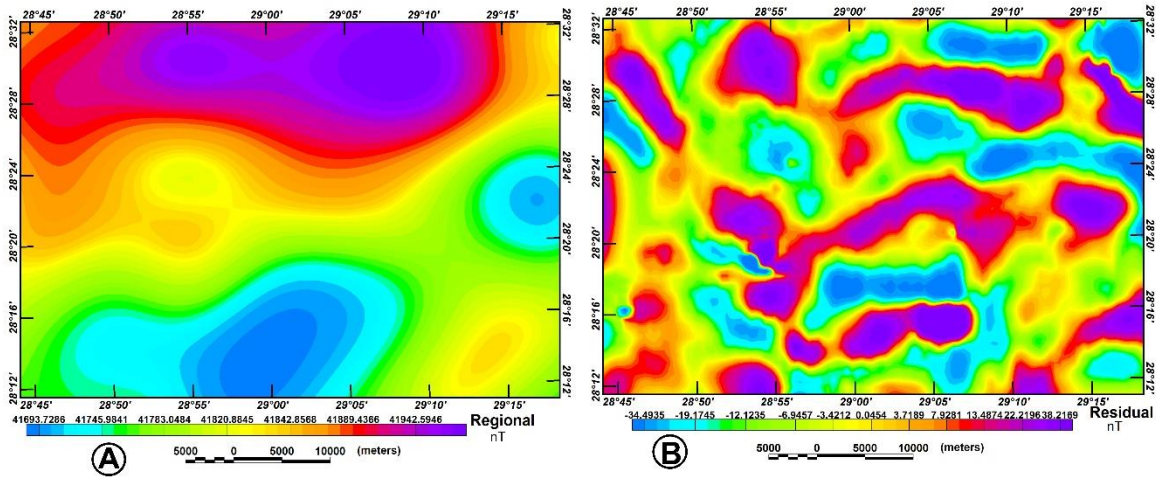

Fig. 14. (A) regional (low-pass) magnetic anomaly map. (B) residuals (high-pass) magnetic anomaly map.

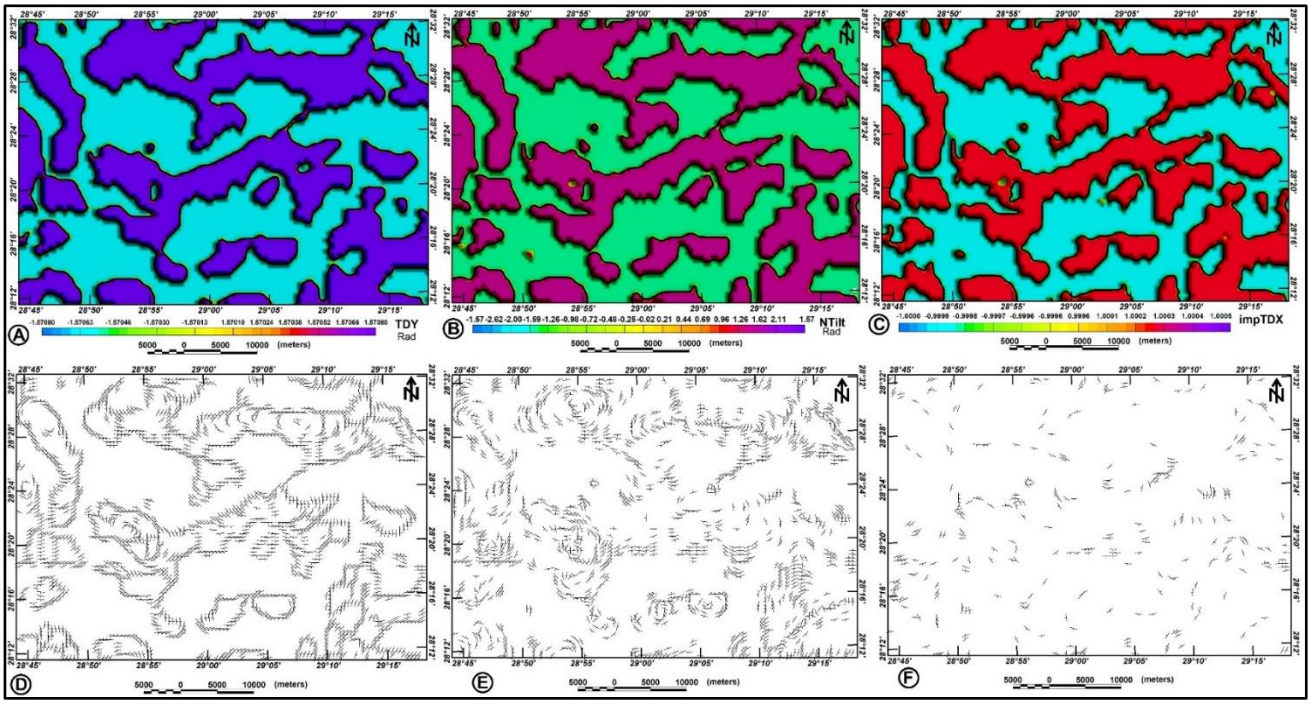

Fig. 15. (A) TDY. (B) NTilt. (C) impTDX filters of the RTP aeromagnetic data show the edges of subsurface causative bodies. The source edge detection lineaments of the TDY, NTilt, and impTDX filters are shown in (D, E, and F), respectively.

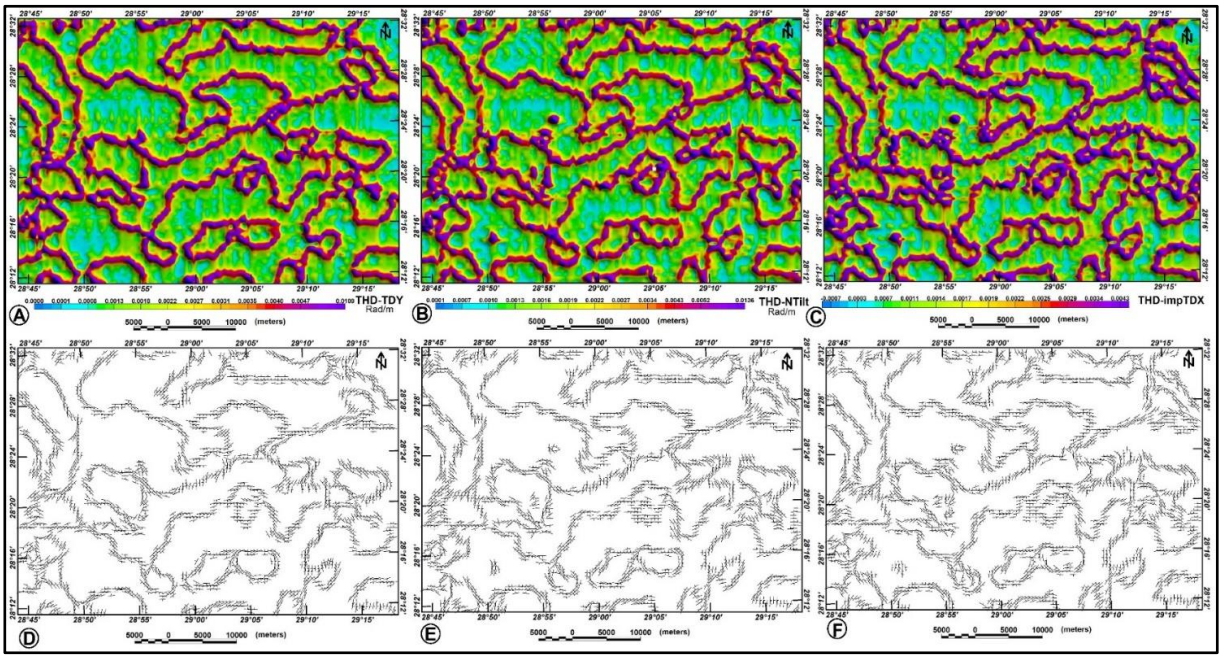

Fig. 16. (A) THD-TDY. (B) THD-NTilt. (C)THD_impTDX filters of the RTP aeromagnetic data show the edges of subsurface causative bodies. The source edge detection lineaments of the THD-TDY, THD-NTilt, and THD_impTDX filters are shown in (D, E, and F), respectively.

indicators for guiding exploration efforts in mineral-rich regions. The intersecting lineaments converge at junction points, which are considered highly favorable locations for potential ore deposits. These intersection zones are often critical in mineral exploration, as they can indicate areas of concentrated mineralization.

The lineaments displayed on the vectorization map correspond closely by the boundaries of the causative source bulks, aligning with the edges of these subsurface structures. This matching strongly suggests that the lineaments, identified as favorable areas for ore accumulation, Accord with the boundaries of the subsurface magnetic sources (Fig. 16C). The extracted line segments were used to create the orientation entropy heat map (Fig. 16D). This map reflects variations in feature orientations, such as lineaments that include intersections and junctions, enabling the identification of areas with structural difficulty.

5. Conclusions

In summary, this research demonstrates the utility of combining remote sensing, GIS, and magnetic geophysical methods to assess the mineral resource potential of the Bahariya-Farafra region. Integrating high-precision edge detection filters and CET grid analysis has enabled detailed mapping of geological structures and identification of mineralized zones, particularly those associated with fault lines and contours. These findings suggest that the region holds substantial untapped mineral resources that could support Egypt's industrial sector and contribute to economic diversification. This study paves the way for targeted exploration efforts and more informed resource management by providing a clearer understanding of the subsurface geology. The methodologies applied here offer a model that can be replicated in similar arid regions to optimize mineral exploration and support sustainable regional development.

References

Abuzied, S.M., Alrefaee, H.A., Khalifa, I.H. (2024). Integrating geospatial and petrographic modeling approach for the discovery of Sulphide-Deposits potential at the El-Kid Region in Egypt. Model. Earth Syst. Environ. 10, 4803–4844. https://doi.org/10.1007/s40808-024-02031-1

Afify A.M., Sanz-Monteroa M.E., Calvo J.P., (2015). Ironstone deposits hosted in Eocene carbonates from Bahariya (Egypt) - New perspective on cherty ironstone occurrences. Sedimentary Geology 329, 81–97.

Afify, A.M., Sanz-Montero, M.E., Calvo, J.P., Wanas, H.A., (2015). Diagenetic origin of ironstone crusts in the Lower Cenomanian Bahariya Formation, Bahariya Depression, Western Desert, Egypt. Journal of African Earth Sciences 101, 333–349.

Alexander, I.O., Samuel, O.O., Esther, C.M., Theophillus, T.E., Kingsley, C.I., Kingsley, C.N. (2015). Integrating Landsat-ETM and Aeromagnetic data for enhanced structural interpretation over Naragwata area, North – Central Nigeria. Int J Sci Eng Res 6(9):2229–5518.

Araffa, S., Alrefaee, H., Nagy, M. (2020). Potential of groundwater occurrence using geoelectrical and magnetic data: A case study from south Wadi Hagul area, the northern part of the Eastern Desert. Egypt. J African Earth Sci. 172:103970. doi:10.1016/j.jafrearsci.2020.103970

Blakely, R. J., (1996) . Potential theory in gravity and magnetic applications. 1st ed. Cambridge, UK: Cambridge University Press, 441p.

El Akkad, S.E., Issawi, B. (1963). Geology and iron ore deposits of Bahariya Oasis. Geological Survey of Egypt 18 (300 pp).

El Ayyat, A.M., (2013). Sedimentology, sequential analysis and claymineralogy of the lower Eocene sequence at Farafra Oasis area, Western Desert of Egypt. Journal of African Earth Sciences 78, 28–50.

El-Badrawy, H.T., Abbas, A.M., Massoud, U., Abu-Alam, T., Alrefaee, H.A., Abo Khashaba, S.M. and Nagy, M., (2024). Integrated approach-based groundwater mapping in sohag governorate, upper Egypt, using remote sensing and aeromagnetic data. *Front. Earth Sci.* 12:1456055. doi: 10.3389/feart.2024.1456055.

Eldosouky, A. M., Abdelkareem, M., Elkhateeb, S. O. (2017). Integration of remote sensing and aeromagnetic data for mapping structural features and hydrothermal alteration zones in Wadi Allaqi area, South Eastern Desert of Egypt. J. Afr. Earth Sci. 130, 2837. https://doi.org/10.1016/j.jafrearsci.2017.03.006 (2017).

Eldosouky, A.M., Abdelkareem, M., Elkhateeb, S.O. (2017) Integration of Remote Sensing and Aeromagnetic Data for Mapping Structural Features and Hydrothermal Alteration Zones in Wadi Allaqi Area, South Eastern Desert of Egypt. J. Afr. Earth Sci. 2017, 130, 28–37.

Eldosouky, A.M., and Elkhateeb, S.O. (2018). Texture Analysis of Aeromagnetic Data for Enhancing Geologic Features Using Co-Occurrence Matrices in Elallaqi Area, South Eastern Desert of Egypt. NRIAG J. Astron. Geophys., 7, 155–161. [Google Scholar] [CrossRef]

Eldosouky, A.M., Eleraki, M., Mansour, A., Saada A. S., Zamzam, S. (2024). Geological controls of mineralization occurrences in the Egyptian Eastern Desert using advanced integration of remote sensing

and magnetic data. Sci Rep 14, 16700. https://doi.org/10.1038/s41598-024-66924-y

Eldosouky, A.M., El-Qassas, R.A.Y., Pham, L.T., Abdelrahman, K., Alhumimidi, M.S., El Bahrawy, A., Mickus, K., Sehsah, H. (2022b). Mapping Main Structures and Related Mineralization of the Arabian Shield (Saudi Arabia) Using Sharp Edge Detector of Transformed Gravity Data. Minerals, 12, 71. https://doi.org/10.3390/min12010071

El-Etr, H.A., Moustafa, A.R., (1978). Field relations of the main basalt occurrences of the Bahariya Region, central Western Desert, Egypt. Proceedings of the Egyptian Academy of Science 31, 191–201.

El-Hussein, M., Shokry, M. (2020). Use of the airborne magnetic data for edge basalt detection in Qaret Had El Bahr area, Northeastern Bahariya Oasis, Egypt. Bull Eng Geol Environ 79:4483–4499

Elkhateeb, S. O., Eldosouky, A. M., Khalifa, M. O., Aboalhassan, M. (2021). Probability of mineral occurrence in the Southeast of Aswan area, Egypt, from the analysis of aeromagnetic data. Arab. J. Geosci. 14, 1514. https://doi.org/10.1007/s12517-021-07997-1.

Floyd F. Sabins, (1999). Remote sensing for mineral exploration. Ore Geology Reviews 14, 157–183.

Holden, E.J., Dentith, M., Kovesi, P. (2008). Towards the automated analysis of regional aeromagnetic data to identify regions prospective for gold deposits. Comput. Geosci., 34, 1505–1513.

Griffin, W. R., (1949). Residual gravity in theory and practice. Geophys J. 14, 39–56. doi:10.1190/1.1437506.

Ibraheem, I.M., Tezkan, B., Ghazala, H., Othman, A.A. (2023). A New Edge Enhancement Filter for the Interpretation of Magnetic Field Data. Pure Appl. Geophys. 180, 2223–2240. doi:10.1007/s00024-023-03249-3

Lowrie, W. (2007). Fundamentals of geophysics, 2nd edn. Cambridge University Press, New York, p 38.

Meneisy, M.Y., 1990. Vulcanicity. In: Said, R. (Ed.), The Geology of Egypt. A.A. Balkema, Rotterdam, pp. 57–172.

Moustafa, A.R., Saoudi, A., Moubasher, A., Ibrahim, I.M., Molokhia, H., Schwartz, B., (2003). Structural setting and tectonic evolution of the Bahariya Depression,Western Desert, Egypt. GeoArabia 8 (1), 91–124.

Nabighian, M.N., Grauch, V.J.S., Hansen, R.O., Lafehr, T.R., Li, Y., Peirc, J.W., Phillips, J.D., Ruder, M.E. (2005). The historical development of the magnetic method in exploration, Society of Exploration. Geophysics 70(6):33ND-61ND. https:// doi. org/ 10. 1190/1.21337 84. (75th Anniversary)

Nasuti A., Nasuti Y., Moghadas D. (2018). Enhancing Potential Field Data Using TDY Filter. In: Near Surface Geoscience Conference. https://doi.org/10.3997/2214-4609.201802747

Nasuti, Y.; Nasuti, A.; Moghadas, D. (2019). STDR: A novel approach for enhancing and edge detection of potential field data. Pure Appl. Geophys. 176, 827–841. doi:10.1007/s00024-018-2016-5

Obaidalla, N.A., El Ayyat, A.M., Kassab, A.S., (2006). Biostratigraphical and sedimentological studies on the Upper Cretaceous/Paleogene sequence,Western Desert, Egypt. Bulletin of Faculty of Science, Assiut University 35 (2), 141–208.

Othman, A.A., Ibraheem, I.M. (2024). Origin of El-Maghara Anticlines, North Sinai Peninsula, Egypt: Insights from Gravity Data Interpretation Using Edge Detection Filters. Arab. J. Sci. Eng. 49, 863–882. doi:10.1007/s13369-023-08225-6

Pham, L.T. (2023). A novel approach for enhancing potential fields: application to the Tuangiao, Vietnam aeromagnetic data. Eur. Phys. J. Plus 138, 1134. https://doi.org/10.1140/epjp/s13360-023-04760-1

Pham, L.T., Oliveira, S.P., Duong, V.H., Abdelrahman, K., Fnais, M.S., Gomez-Ortiz, D., Nguyen, D.V., VO, Q.T., Duy, T.K., Eldosouky, A.M. (2023). Aeromagnetic data interpretation of the northern Kontum massif (Vietnam) for mapping subsurface structures, Geocarto International. 38:1, doi:10.1080/10106049.2023.2246940

Rabeh, T., Bedair, S., Abdel Zaher, M. (2018). Structural control of hydrogeological aquifers in the Bahariya Oasis Western Desert, Egypt. Geosci J 22(1):145–154

Said, R., (1962). The Geology of Egypt. Elsevier, Amsterdam (377 pp).

Said, R., Issawi, B., (1964). Geology of the northern plateau, Bahariya Oasis, Egypt. Geological Survey of Egypt 29 (41 pp).

Sanz-Montero, M.E., Wanas, H., Muñoz-García, M.B., González-Acebrón, L., López, M.V., (2013). The uppermost deposits of the stratigraphic succession of the Farafra Depression (Western Desert, Egypt): evolution to a Post-Eocene continental event. Journal of African Earth Sciences 87, 33–43.

Sehim, A.A., (1993). Cretaceous tectonics in Egypt. Egyptian Journal of Geology 371, 335–372.

Shebl, A., Abdellatif, M., Elkhateeb, S.O., Csámer, Á. (2021). Multisource Data Analysis for Gold Potentiality Mapping of Atalla Area and Its Environs, Central Eastern Desert, Egypt. Minerals, 11, 641. https://doi.org/10.3390/ min11060641

Spector, A., and Grant, F.S. (1970). Statistical models for interpreting aeromagnetic data. Geophysics, 35, 293–302.

دمج الاستشعار عن بُعد ونظم المعلومات الجغرافية والجيولوجيا المغناطيسية لتقييم الموارد المعدنية في منطقة الواحات البحرية – الفرافرة بالصحراء الغربية، مصر، من أجل التنمية الصناعية

آلاء نايف[1]، ومصطفى ناجي[2]، ومحمد أنور أحمد[1]، وأحمد المصلحى السيد[3]

[1] الهيئة القومية للاستشعار من البُعد وعلوم الفضاء، القاهره، جمهورية مصر العربية

[2] قسم الجيولوجيا، كلية العلوم، جامعة كفر الشيخ، جمهورية مصر العربية

[3] قسم العلوم الجيوفيزيقية، المركز القومي للبحوث، القاهرة، جمهورية مصر العربية

تهدف هذه الدراسة إلى دمج تقنيات الاستشعار عن بُعد، ونظم المعلومات الجغرافية، والطريقة الجيوفيزيائية المغناطيسية الجوية لتقييم الموارد المعدنية في منطقة الواحات البحرية – الفرافرة بالصحراء الغربية في مصر، لتعزيز التنمية الصناعية المستدامة. تُعد المنطقة غنية بالعديد من المعادن اللافلزية والأحجار الزخرفية، بما في ذلك الكالسيت، والجبس، والمعادن الطينية، والحجر الرملي، والحجر الجيري، والدولوميت، بالإضافة إلى رواسب مهمة من خام الحديد. تم استخدام فلاتر الكشف الحدي المتقدمة وتحليل شبكة CET على البيانات المغناطيسية الجوية لتحديد الهياكل الجيولوجية، وأنظمة الصدوع، والمناطق ذات الاحتمالية العالية للتعدين. أظهرت النتائج مناطق واعدة للمعادن المحتوية على الكبريتيد، مدعومة بتحديد خطوط رئيسية مرتبطة بتراكم المعادن. يوفر هذا النهج الشامل رؤى قيمة للاستثمار في الصناعات الاستراتيجية، ويعزز الدخل القومي، ويشجع على التنمية الحضرية، مما يساهم في تخفيف مشكلات الكثافة السكانية في المراكز الحضرية. تؤكد الدراسة على أهمية المنهجيات متعددة التخصصات في تقييم الموارد، مما يمهد الطريق لمبادرات استكشاف مستقبلية وتنمية مستدامة في الصحراء الغربية بمصر.